Olefin Polymerization with Homogeneous Ziegler−Natta Catalysts: A DFT Quantum-Mechanical Study of the Reactions of Cp_2MtCH_3Cl Complexes (Mt = Ti, Zr) with $Al(CH_3)_3$ and MAO

Roberto Fusco,* Luca Longo, Francesco Masi, and Fabio Garbassi

Centro Ricerche Novara "Istituto Guido Donegani", EniChem S.p.A., Via Fauser, 4, 28100 Novara, Italy

Received June 12, 1997; Revised Manuscript Received September 11, 1997[⊗]

ABSTRACT: The reactions of $Cp_2MtMeCl$ ($Cp = \eta_5$-C_5H_5, Mt = Ti, Zr, Me = CH_3) with $AlMe_3$ and with $MeAl[OAl_2H_4]_2O$, as a model of the cocatalytic site of methylalumoxane (MAO), were studied by means of DFT quantum-mechanical calculations. The energy required to form the Cp_2MtMe^+ cation from dissociation of $Cp_2MtMeCl{\cdot}AlMe_3$ and different kinds of chlorine-bridged and oxygen-bridged $Cp_2MtMeCl{\cdot}$MAO model adducts accounts for the higher cocatalytic activity exhibited by methylalumoxane with respect to $AlMe_3$ in olefin polymerization. Both the presence of highly acidic aluminum atoms and negative charge dispersion power of $XMAO^-$ macroanions (X = Cl, Me) are essential features in determining low dissociation energies. Possible key roles played by monomer and $AlMe_3$ content of MAO in affecting active species formation are suggested. The computational results support the idea that, in the absence of degradative side reactions, titanium and zirconium MAO-based systems should exhibit comparable catalytic activity.

Introduction

The discovery that group IVB metallocene complexes, in the presence of chloroalkylaluminum compounds, react with ethylene, to give high molecular weight linear polyethylene, dates back to 1957.[1] However, the extremely higher productivity exhibited by traditional $TiCl_4/Al(C_2H_5)_3$ heterogeneous Ziegler−Natta catalysts and their ability to react also with α-olefins to give highly stereoregular polymers[2] eclipsed for many years the interest for metallocene-based catalysis.

About 20 years later, the research in the field of homogeneous catalysis was greatly stimulated by the discovery that methylalumoxane (MAO) is able to activate metallocene complexes, increasing by several orders of magnitude their ability to polymerize ethylene and α-olefins with high yields.[3]

Despite the growing industrial interest for these systems and the great efforts made to clarify the role played by methylalumoxane in the activation process,[4] many questions still remain unanswered. The amorphous structure of MAO and its chemical fluxionality make it and the chemical reactions occurring when it is mixed with metallocenes to form catalytically active systems extremely difficult to study. It is believed that methyalumoxane is involved in several reactions:[5] (i) alkylation of metallocene (in the case of dihalogenated precursors);[6a] (ii) formation of "cationlike" active species;[6b] (iii) deactivation of catalyst poisons.

Concerning step ii, it is generally assumed that the main role played by aluminum-based cocatalysts should consist of the extraction of the X^- anion (X = halogen or alkyl group) from a neutral alkylated metallocene precursor L_2MtRX[6] (L = cyclopentadienyl ligand, R = alkyl group) to form ion pairs in which alkylated cationic metallocenes L_2MtR^+ should be responsible for olefin polymerization.[7] In this framework, the high efficiency of MAO is generally ascribed both to its strong Lewis acidity, making it a good anion-extractor, and to its ability to form a weakly coordinating $X{\cdot}MAO^-$ macroanion.[8]

In the last few years we used molecular modeling techniques, combined with spectroscopic investigations and polymerization tests, to identify the main structural features of MAO accounting for its high cocatalytic activity.[9]

In previous papers[9,10] we put in evidence, on the basis of energy calculations, the idea that ion pair separation could play a critical role in determining the activity of metallocene-based catalytic systems. With $Cp_2TiMeCl/AlMe_2Cl$ ($Cp = \eta_5$-C_5H_5, Me = CH_3) system, the high energy (> 100 kcal/mol) required to separate Cp_2TiMe^+ from $AlMe_2Cl_2^-$ in vacuum can hardly be compensated for by the solvation energy in the weakly polar solvents usually used in polymerization (15−30 kcal/mol).[11] We suggested that olefin separated ion pairs (OSIP) $Cp_2TiMe^+/C_2H_4/AlMe_2Cl_2^-$, where an ethylene molecule is sandwiched between the cation and the anion, represent, in that case, the least unfavorable way to allow olefin coordination and following insertion into the metal-carbon bond.[10]

In the present work we made an effort to rationalize theoretical considerations and experimental observations collected in recent years, by building different models of the "cocatalytic site" of MAO, simulating their reaction with typical titanocene and zirconocene catalytic precursors, and investigating cationic active species formation in comparison with those obtained from metallocene/trimethylaluminum systems.

Models of the Cocatalytic Sites in MAO

Different hypothesis about methylalumoxane structure have been formulated[4,8,12−13] on the basis of experimental evidences coming from various characterization techniques[13] as well as from studies of model compounds with well defined structure.[8a,13]

It is not the aim of this paper to present a review of all the MAO models suggested until now but to propose a new model of cocatalytic site of MAO including all the main features supposed to be relevant to explain its cocatalytic behavior.

The idea of MAO simply conceived as an ensemble of linear $[-Al(CH_3)O-]_n$ oligomers is quite unrealistic for at least two reasons:

[⊗] Abstract published in *Advance ACS Abstracts,* November 15, 1997.

S0024-9297(97)00861-9 CCC: $14.00

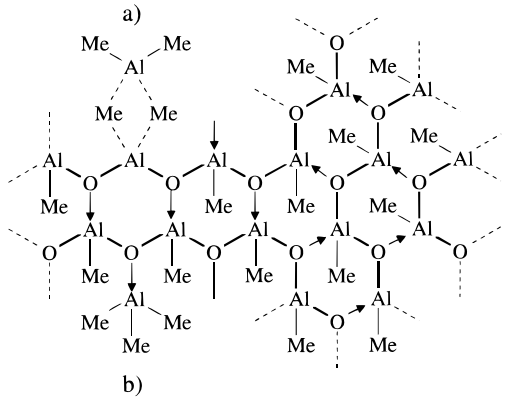

Figure 1. Possible aggregation of methylalumoxane chains. The arrows denote O→Al dative bonds between different alumoxanic chains. Two possible ways of coordination of $AlMe_3$ to methylalumoxane are shown: through a double methyl bridge (a) and oxygen coordination (b).

First, aluminum atoms are generally more stable in the tetrahedral rather than in the trigonal planar configuration because of the reactivity of their 3p unoccupied orbital; in fact, the presence of tricoordinated aluminum atoms is peculiar to compounds with sterically hindering substituents of the aluminum, which inhibit the formation of dimeric or oligomeric structures,[14] as well as of metastable transient structures.[15]

Second, tricoordinated aluminum atoms (acidic sites) and dicoordinated oxygen atoms (basic sites) have a high tendency to form O→Al dative bonds, causing the aggregation of the oligomeric chains, giving structures characterized by tetracoordination of aluminum atoms and tricoordination of oxygen atoms (Figure 1); such a situation is very common in many methylalumoxane analogues with well-defined structure.[13]

Furthermore, in contrast to the idea of MAO as a strong Lewis acid, tricoordinated aluminum atoms bridging dicoordinated oxygen atoms are expected to have lower Lewis acidity than that of monomeric trimethylaluminum, because of the p-electron back-donation from oxygen to aluminum.[16]

Although the real coordinative situation of Al and O atoms in MAO is controversal, it can be reasonably assumed that the $[-Al(Me)O-]_n$ chains can aggregate with each other[13] and this is confirmed by experimental evidence, mainly arising from NMR studies.[15,17]

It has been also well established that the presence of "free trimethylaluminum" in MAO[18a] (about 30−40% in the commercial product[8a]) is crucial for the exhibition of a high catalytic activity.[18b,c] It can be reasonably assumed that $AlMe_3$ is at least partly coordinated to alumoxane chains[12,19] through methyl bridges (Figure 1a), or through direct coordination to oxygen atoms (Figure 1b).[18d]

Our model of the cocatalytic site of MAO takes into account all these experimental observations and modelistic considerations, assuming that (a) aluminum atoms are able to interact with metallocene neutral precursors only in the metastable tricoordinated situations;[8,20] (b) aluminum atoms weakly coordinating $AlMe_3$ molecules (Figure 1a) have a higher probability to produce such a situation rather than those involved in inter or intrachain O→Al dative bonds (Figure 1), for both thermodynamic (the higher energy requirements expected to break O−Al bridges compared to that needing to break AlMe--Al bridges) and kinetic factors (dissociation processes involving small molecules like $AlMe_3$ are faster than those impling cooperative rearrangements of macromolecular chains); (c) tricoordinated aluminum atoms bridging two tricoordinated oxygen atoms are expected to be strongly acidic because the p-electron back-donation from oxygen to aluminum should be at least partially inhibited.

$MeAl[OAl_2Me_4]_2O$ can be proposed as a minimal model of the cocatalytic site satisfying the above requisites: it can be considered as the aggregation product of trimeric $Me_2AlOAl(Me)OAlMe_2$ and dimeric $Me_2AlOAlMe_2$ methylalumoxane chain fragments (Figure 2). The formation of two dative O→Al bonds between the two oxygen atoms of the trimer and the two aluminum atoms of the dimer gives a six-membered ring structure. According to point c, the Al* aluminum atom is symmetrically coordinated to two tricoordinated oxygen atoms. To further reduce the complexity of the model, the terminal methyl groups were replaced with hydrogen atoms: in the following we will refer to this model molecule as $MeAl[OAl_2H_4]_2O$ or MAO^H (**1**).

Model Reactions Involved in Active Species Formation

Reactions of $Cp_2MtMeCl$ (Mt = Ti, Zr) with $AlMe_3$, taken as reference cocatalyst, and with different models of cocatalytic sites derived from the MAO^H, were investigated. The choice of prealkylated metallocenes as the starting compounds was made in order to skip the study of the alkylation step. The proposed reactions

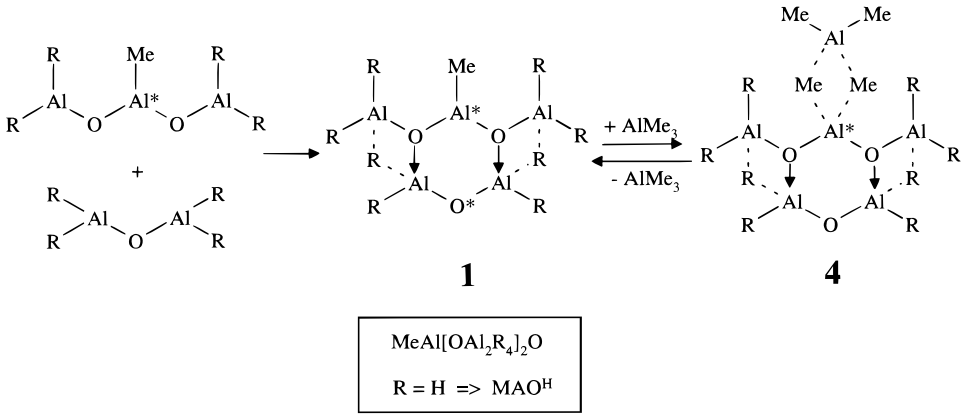

Figure 2. Simplified MAO model, obtained by aggregation between dimeric and trimeric alumoxane chain fragments, in equilibrium with $AlMe_3$. R = H denotes the MAO^H model. The tricoordinated Al* atom in the central structure represents the cocatalytic site.

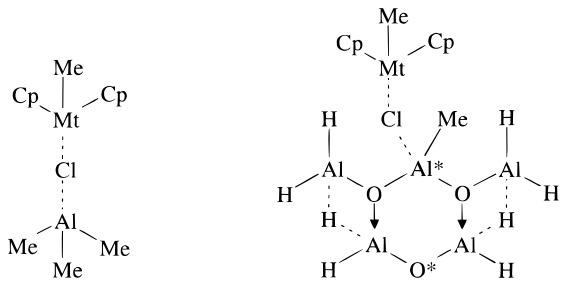

6 **7**

Figure 3. Schematic drawings of $Cp_2MtMeCl{\cdot}AlMe_3$ (**6**) and $Cp_2MtMeCl{\cdot}MAO^H$ (**7**) adducts.

involved in active species formation can be indicated in the following way: (i) reaction between chloroalkylated metallocene and cocatalytic species with formation of Mt−Cl−Al chlorine-bridged adducts; (ii) dissociation of these adducts into free ion pairs; (iii) formation of oxygen-coordinated metallocene/MAO^H adducts; (iv) formation of ion pairs from dissociation of these adducts; (v) stabilization of ion pairs through the formation of metallocene/monomer cationic complexes and counterion/$AlMe_3$ adducts.

It is well-known that trimethylaluminum exists in a dimeric form, $[AlMe_3]_2$[14] (**2**), that is supposed to be in fast equilibrium with the monomeric form **3**:

$$\underset{\mathbf{2}}{[AlMe_3]_2} \rightleftarrows 2\underset{\mathbf{3}}{AlMe_3} \quad (1)$$

In close analogy with reaction 1 we supposed that, according to point b, a double-methyl-bridged trimethylaluminum/methylalumoxane adduct, simulated by $Me_2Al[Me]_2Al[OAl_2H_4]_2O$ (**4**), is in equilibrium with dissociated MAO^H and $AlMe_3$ (Figure 2), as described by reaction 2. The coordination of $AlMe_3$ to the dicoordinated oxygen atom O* in MAO^H (Figure 2), although supposed to be thermodynamically favored with respect to the formation of **4**, will be temporarily neglected because it does not involve the Al* atom directly. This reaction will be explicitely considered in the following section, when the stabilizing effect of trimethylaluminum on active species formation will be investigated.

$$\underset{\mathbf{4}}{Me_2Al[Me]_2Al[OAl_2H_4]_2O} \rightleftarrows \underset{\mathbf{1}}{MeAl[OAl_2H_4]_2O} + AlMe_3 \quad (2)$$

$Cp_2MtMeCl$ catalytic precursors (**5**) are supposed to react with $AlMe_3$ or MAO^H to give respectively $Cp_2MtMe{\cdot}ClAlMe_3$ (**6**) and $Cp_2MtMe{\cdot}ClMeAl[OAl_2H_4]_2O$ (**7**) adducts (Figure 3):

$$\underset{\mathbf{5}}{Cp_2MtMeCl} + \underset{\mathbf{3}}{AlMe_3} \rightarrow \underset{\mathbf{6}}{Cp_2MtMe{\cdot}ClAlMe_3} \quad (3)$$

$$\underset{\mathbf{5}}{Cp_2MtMeCl} + \underset{\mathbf{1}}{MeAl[OAl_2H_4]_2O} \rightarrow \underset{\mathbf{7}}{Cp_2MtMe{\cdot}ClMeAl[OAl_2H_4]_2O} \quad (4)$$

The heterolytic dissociation of the Mt−Cl bond in **6** and **7** leads to the formation of free cation/anion pairs:

$$\underset{\mathbf{6}}{Cp_2MtMe{\cdot}ClAlMe_3} \rightarrow \underset{\mathbf{8}}{Cp_2MtMe^+} + \underset{\mathbf{9}}{ClAlMe_3^-} \quad (5)$$

$$\underset{\mathbf{7}}{Cp_2MtMe{\cdot}ClMeAl[OAl_2H_4]_2O} \rightarrow \underset{\mathbf{8}}{Cp_2MtMe^+} + \underset{\mathbf{10}}{ClMeAl[OAl_2H_4]_2O^-} \quad (6)$$

Both dissociations (eqs 5 and 6) imply charge separation and are expected to require high energy in weakly polar solvents. It has been suggested that ion pair separation can be greatly facilitated by the ability of the $XMAO^-$ macroanion to delocalize the negative charge,[8c] as this feature is closely related to its size. Because of the difficulty of simulating such a macromolecular structure, the charge delocalization occurring in an infinitely large virtual anion was simulated by neutralizing the negative charge of the anion **10**. To this aim a cationic model of MAO was introduced, $MeAl[OAl_2H_4]_2O{\cdot}AlH_2^+$ ($MAO^H{\cdot}AlH_2^+$ (**11**)), obtained by coordinating the AlH_2^+ cation to O* of MAO^H (Figure 4). The reaction of $Cp_2MtMeCl$ with **11** produces the chlorine bridged adduct **12**:

$$Cp_2MtMeCl + \underset{\mathbf{11}}{MeAl[OAl_2H_4]_2O{\cdot}AlH_2^+} \rightarrow \underset{\mathbf{12}}{Cp_2MtMe{\cdot}ClMeAl[OAl_2H_4]_2O{\cdot}AlH_2^+} \quad (7)$$

that can dissociate as

$$\underset{\mathbf{12}}{Cp_2MtMe{\cdot}ClMeAl[OAl_2H_4]_2O{\cdot}AlH_2^+} \rightarrow Cp_2MtMe^+ + \underset{\mathbf{13}}{ClMeAl[OAl_2H_4]_2O{\cdot}AlH_2} \quad (8)$$

forming the $Cp_2MtMe^+/ClMeAl[OAl_2H_4]_2O{\cdot}AlH_2$ "virtual ion pair". Because the "virtual anion" **13** is a neutral species, no charge separation occurs in such a reaction and lower dissociation energies are expected.

In the following section, reactions involving both neutral MAO^H and cationic $MAO^H{\cdot}AlH_2^+$ models will be investigated.

Concerning the possible role of methylalumoxane as solvating agent of ion pairs, it has been suggested the cationic active species could be stabilized by weak interactions with oxygen atoms of alumoxane chains[15,21] as shown in Figure 5. The thermodynamics of migration of Cp_2MtMe^+ cations along the alumoxane chain to form oxygen-coordinated Mt−O adducts, as well as their dissociation, can be studied in order to check this hypothesis. In the idea that almost all the oxygen atoms in methylalumoxane form O→Al dative bonds, thus making them unavailable for Cp_2MtMe^+ coordination, the remaining oxygen atoms, coordinating trimethylaluminum molecules, have a higher probability to react with metallocene cations.

In this framework the cation migration can be better conceived as an exchange reaction between Cp_2MtMe^+, initially bound to Al* through a chlorine bridge, and an $AlMe_3$ molecule coordinated to an oxygen atom of methylalumoxane (Figure 5). When such an exchange occurs, the formation of free Cp_2MtMe^+ cations implies the breaking of Mt−O bonds. Obviously the above mentioned ability of $XMAO^-$ macroanions in delocalizing the negative charge can affect the strength of these bonds. Therefore also in this case two limit situations were considered.

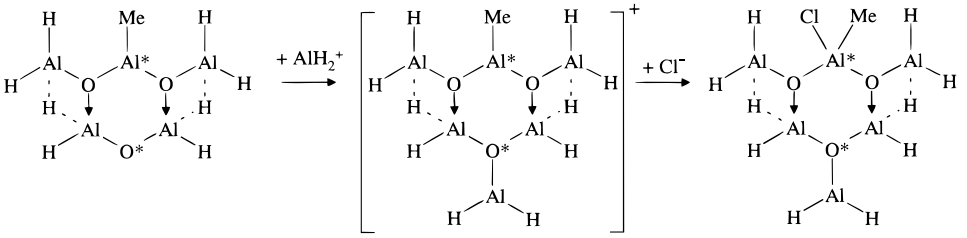

1 **11** **13**

Figure 4. Cationic $MAO^{H}\cdot AlH_2^+$ (**11**) model and $ClMAO^{H}\cdot AlH_2$ (**13**) virtual anion

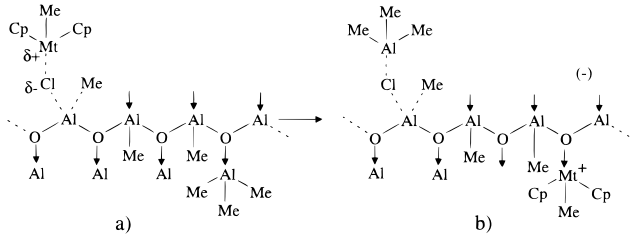

Figure 5. Possible migration mechanism of Cp_2MtMe^+ cations from the chlorine atom of the initial adduct (a) to an oxygen atom of the alumoxanic chain and (b), that paralleled by migration of an $AlMe_3$ molecule in the opposite direction.

For the neutral MAO^{H} model the migration of the cationic metallocene toward O* was studied, flanked by $AlMe_3$ migration from O* to Cl:

$$\underset{\mathbf{14}}{Cp_2MtMe\cdot ClMeAl[OAl_2H_4]_2O\cdot AlMe_3} \rightarrow \underset{\mathbf{15}}{Me_3Al\cdot ClMeAl[OAl_2H_4]_2O\cdot MtCp_2Me} \quad (9)$$

For the cationic $MAO^{H}\cdot AlH_2^+$ model, the exchange reaction (eq 10) between Cp_2MtMe^+ coordinated to the Cl atom of the virtual anion $ClMeAl[OAl_2H_4]_2O\cdot AlH_2$ and $AlMe_3$ coordinated to O* of MAO^{H} was investigated, assuming that, from an electronic point of view, the oxygen atoms of an infinitely large macroanion are virtually indistinguishable from O* in the neutral MAO^{H}:

$$\underset{\mathbf{12}}{Cp_2MtMe\cdot ClMeAl[OAl_2H_4]_2O\cdot AlH_2^+} + \underset{\mathbf{16}}{MeAl[OAl_2H_4]_2O\cdot AlMe_3} \rightarrow \underset{\mathbf{17}}{MeAl[OAl_2H_4]_2O\cdot MtCp_2Me^+} + \underset{\mathbf{18}}{Me_3Al\cdot ClMeAl[OAl_2H_4]_2O\cdot AlH_2} \quad (10)$$

The dissociation of the Mt−O bonds in the neutral and cationic adducts **15** and **17** was investigated by studying the following reactions:

$$\underset{\mathbf{19}}{ClMeAl[OAl_2H_4]_2O\cdot MtCp_2Me} \rightarrow \underset{\mathbf{8}}{Cp_2MtMe^+} + \underset{\mathbf{10}}{ClMeAl[OAl_2H_4]_2O^-} \quad (11)$$

$$\underset{\mathbf{17}}{MeAl[OAl_2H_4]_2O\cdot MtCp_2Me^+} \rightarrow \underset{\mathbf{8}}{Cp_2MtMe^+} + \underset{\mathbf{1}}{MeAl[OAl_2H_4]_2O} \quad (12)$$

In reaction 11, where adducts **19** were considered instead of **15**, the absence of $AlMe_3$ coordinated to the Cl atom is assumed to be not relevant in determining the Mt−O bond dissociation energy.

According to Cossee's mechanism,[22] the formation of the coordinatively insatured cations **8** is essential to allow olefin coordination to the transition metal and the successive insertion into the metal−carbon bond. The energy produced by the coordination of ethylene to Cp_2MtMe^+ complexes was also calculated:

$$\underset{\mathbf{8}}{Cp_2MtMe^+} + C_2H_4 \rightarrow \underset{\mathbf{20}}{Cp_2MtMe(C_2H_4)^+} \quad (13)$$

Although such an intermediate has never been experimentally observed, being a transient species, it is expected that ethylene coordination produces a stabilizing effect on the Cp_2MtMe^+ cation, similar to that arising from its interaction with an aromatic solvent molecule.

Further thermodynamic stabilization of dissociated ion pairs could derive from trimethyaluminum coordination to the residual chlorine atom of the counterion. The coordination energy was calculated for the counterions obtained starting from the three cocatalysts $AlMe_3$, MAO^{H}, and $MAO^{H}\cdot AlH_2^+$, as described by the following reactions:

$$\underset{\mathbf{3}}{AlMe_3} + \underset{\mathbf{9}}{ClAlMe_3^-} \rightarrow \underset{\mathbf{21}}{[AlMe_3]_2Cl^-} \quad (14)$$

$$\underset{\mathbf{3}}{AlMe_3} + \underset{\mathbf{10}}{ClMeAl[OAl_2H_4]_2O^-} \rightarrow \underset{\mathbf{22}}{AlMe_3\cdot ClMeAl[OAl_2H_4]_2O^-} \quad (15)$$

$$\underset{\mathbf{3}}{AlMe_3} + \underset{\mathbf{13}}{ClMeAl[OAl_2H_4]_2O\cdot AlH_2} \rightarrow \underset{\mathbf{18}}{Me_3Al\cdot ClMeAl[OAl_2H_4]_2O\cdot AlH_2} \quad (16)$$

The same stabilizing effect on ion pair dissociation can arise from $AlMe_3$ coordination to oxygen atoms of **10** and **1** coming out from the dissociation of the Mt−O bond, respectively, of **15** (or **19**) and **17**, as described by reactions 17 and 18.

$$\underset{\mathbf{3}}{AlMe_3} + \underset{\mathbf{10}}{ClMeAl[OAl_2H_4]_2O^-} \rightarrow \underset{\mathbf{23}}{ClMeAl[OAl_2H_4]_2O\cdot AlMe_3^-} \quad (17)$$

$$\underset{\mathbf{3}}{AlMe_3} + \underset{\mathbf{1}}{MeAl[OAl_2H_4]_2O} \rightarrow \underset{\mathbf{16}}{MeAl[OAl_2H_4]_2O\cdot AlMe_3} \quad (18)$$

Table 1. Nomenclature Adopted for MAO^H Adducts

	Cocatalytic Precursor and Lewis Acids	
4	$Me_2Al[Me]_2Al[OAl_2H_4]_2O$	$Me_3Al{\cdot}MAO^H$
1	$MeAl[OAl_2H_4]_2O$	MAO^H
11	$MeAl[OAl_2H_4]_2O{\cdot}AlH_2^+$	$MAO^H{\cdot}AlH_2^+$
	Chlorine-Bridged Metallocene/Aluminum Adducts	
7	$Cp_2MtMe{\cdot}ClMeAl[OAl_2H_4]_2O$	$Cp_2MtMe{\cdot}ClMAO^H$
12	$Cp_2MtMe{\cdot}ClMeAl[OAl_2H_4]_2O{\cdot}AlH_2^+$	$Cp_2MtMe{\cdot}ClMAO^H{\cdot}AlH_2^+$
14	$Cp_2MtMe{\cdot}ClMeAl[OAl_2H_4]_2O{\cdot}AlMe_3$	$Cp_2MtMe{\cdot}ClMAO^H{\cdot}AlMe_3$
	Chlorinated Counterions	
10	$ClMeAl[OAl_2H_4]_2O^-$	$ClMAO^{H-}$
13	$ClMeAl[OAl_2H_4]_2O{\cdot}AlH_2$	$ClMAO^H{\cdot}AlH_2$
	Oxygen-Coordinated Metallocene/Aluminum Adducts	
19	$ClMeAl[OAl_2H_4]_2O{\cdot}MtCp_2Me$	$ClMAO^H{\cdot}MtCp_2Me$
17	$MeAl[OAl_2H_4]_2O{\cdot}MtCp_2Me^+$	$MAO^H{\cdot}MtCp_2Me^+$
15	$Me_3Al{\cdot}ClMeAl[OAl_2H_4]_2O{\cdot}MtCp_2Me$	$Me_3Al{\cdot}ClMAO^H{\cdot}MtCp_2Me$
	Trimethylaluminum-Stabilized Counterions	
22	$Me_3Al{\cdot}ClMeAl[OAl_2H_4]_2O^-$	$Me_3Al{\cdot}ClMAO^{H-}$
18	$Me_3Al{\cdot}ClMeAl[OAl_2H_4]_2O{\cdot}AlH_2$	$Me_3Al{\cdot}ClMAO^H{\cdot}AlH_2$
23	$ClMeAl[OAl_2H_4]_2O{\cdot}AlMe_3^-$	$ClMAO^H{\cdot}AlMe_3^-$
16	$MeAl[OAl_2H_4]_2O{\cdot}AlMe_3$	$MAO^H{\cdot}AlMe_3$

Density Functional Calculations

All the calculations were performed using the DMol 4.0.0 program[23] (Molecular Simulations Inc.) based on the density functional theory.[24] The electronic configurations of the molecular systems were described by restricted double-numerical basis sets without polarization functions. The $1s^2$ configuration on carbon and aluminum, $1s^2$ and $2s^2$ on aluminum and chlorine, $1s^2$ $2s^2$ $2p^6$ on titanium, and $1s^2$ $2s^2$ $2p^6$ $3s^2$ $3p^6$ $3d^{10}$ on zirconium were assigned to the core and treated by the frozen-core approximation. For each molecule studied, a geometry optimization was carried out with C_s symmetry constraint, using the BFGS energy minimization algorithm.[25] The Vosko−Wilk−Nusair[26] (VWN) local correlation parameters (LDA) were applied to evaluate the density functionals. The computations were also performed recalculating the energies of the VWN optimized structures both with single point gradient-corrected self-consistent calculations, using Perdew−Wang−Becke[27] (PWB) potentials, including polarization functions, and with a further reoptimization in the nonlocal density approximation (NLDA). In a previous paper[10] the comparison of the experimental polymerization enthalpy of ethylene[28] (−22.3 kcal/mol) with the olefin insertion energies, calculated at the LDA level (−30.7 kcal/mol) and the NLDA level (−20.6 kcal/mol), showed a tendency opposite of that the former method to overestimate and of the latter to underestimate the experimental value. In the present work, in the only case where a direct comparison with experimental data was possible (19 kcal/mol for the dissociation enthalpy of dimeric $AlMe_3$[29]) was a better agreement obtained with calculations performed at LDA level (19.8 kcal/mol) rather than with application of the gradient correction (7.9 kcal/mol for the reoptimized structures). Although this occurrence could be casual, because the general trend of the reaction energies remains qualitatively the same for both methodologies, we chose to base the discussion on the results obtained at LDA level (Tables 2 and 3). However, we have also reported for completeness the reaction energies calculated through structure reoptimization, including the gradient correction (Tables 4 and 5).

Results and Discussion

For the sake of simplicity we adopted a more condensed symbology to identify the different MAO^H adducts. It is simply based on the replacement of $MeAl[OAl_2H_4]_2O$ moiety with the symbol "MAO^H" in the general formula, as reported in Table 1.

Table 2. Binding Energies (kcal/mol) of the Examined Intermediates Calculated at the LDA Level

	Group A. Cocatalytic Precursors and Lewis Acids (Figure 6)		
2	$[AlMe_3]_2$		−2468.2
4	$Me_2Al[Me]_2Al[OAl_2H_4]_2O$		−2987.6
3	$AlMe_3$		−1224.2
1	$MeAl[OAl_2H_4]_2O$		−1739.9
	Group B. Metallocene Complexes (Figure 7)		
		Mt = Ti	Mt = Zr
5	$Cp_2MtMeCl$	−3172.7	−3208.9
8	Cp_2MtMe^+	−2928.2	−2956.9
20	$Cp_2MtMe(C_2H_4)^+$	−3566.3	−3601.7
	Group C. Chlorine-Bridged Metallocene/ Aluminum Adducts (Figures 8 and 11)		
		Mt = Ti	Mt = Zr
6	$Cp_2MtMe{\cdot}ClAlMe_3$	−4408.4	−4439.7
7	$Cp_2MtMe{\cdot}ClMeAl[OAl_2H_4]_2O$	−4936.6	−4970.8
12	$Cp_2MtMe{\cdot}ClMeAl[OAl_2H_4]_2O{\cdot}AlH_2^+$	−5004.6	−5036.9
14	$Cp_2MtMe{\cdot}ClMeAl[OAl_2H_4]_2O{\cdot}AlMe_3$	−6199.3	−6232.5
	Group D. Chlorinated Counterions (Figure 9)		
9	$ClAlMe_3^-$		−1355.9
10	$ClMeAl[OAl_2H_4]_2O^-$		−1906.5
13	$ClMeAl[OAl_2H_4]_2O{\cdot}AlH_2$		−2036.0
	Group E. Oxygen-Coordinated Metallocene/ Aluminum Adducts (Figures 10 and 11)		
		Mt = Ti	Mt = Zr
19	$ClMeAl[OAl_2H_4]_2O{\cdot}MtCp_2Me$	−4957.6	−4997.1
17	$MeAl[OAl_2H_4]_2O{\cdot}MtCp_2Me^+$	−4720.9	−4758.6
15	$Me_3Al{\cdot}ClMeAl[OAl_2H_4]_2O{\cdot}MtCp_2Me$	−6192.7	−6231.0
	Group F. Trimethylaluminum-Stabilized Counterions (Figure 12)		
21	$Cl[AlMe_3]_2^-$		−2604.6
22	$Me_3Al{\cdot}ClMeAl[OAl_2H_4]_2O^-$		−3145.6
18	$Me_3Al{\cdot}ClMeAl[OAl_2H_4]_2O{\cdot}AlH_2$		−3269.6
23	$ClMeAl[OAl_2H_4]_2O{\cdot}AlMe_3^-$		−3174.2
16	$MeAl[OAl_2H_4]_2O{\cdot}AlMe_3$		−2999.2
	Cl^-		−83.6
	C_2H_4		−616.0

In Figures 6−12 the optimized structures of all the compounds examined are presented in homogeneous groups: the cocatalytic precursors and the correspondent Lewis acids (Figure 6); the metallocene complexes (Figure 7); the chlorine-bridged metallocene/cocatalyst adducts (Figure 8); the counterions produced by heterolytic dissociation of the Mt−Cl bond (Figure 9); the oxygen-coordinated metallocene/cocatalyst adducts (Figure 10); the metallocene/MAO^H/$AlMe_3$ adducts (Figure 11); the $AlMe_3$-stabilized counterions (Figure 12). Calculated binding energies of these compounds are reported in Table 2, adopting the same classification criterium. On the basis of these energy values, enthalpies of reactions 1−18 were estimated in terms of the energy difference (ΔE) between products and reagents and summarized in Table 3.

Cocatalytic Precursors and Lewis Acids

On the left side of Figure 6 are reported the optimized structures of the cocatalytic precursors $[AlMe_3]_2$ (**2**) and $Me_3Al{\cdot}MAO^H$ (**4**). The correspondent Lewis acids ($AlMe_3$ (**3**) and MAO^H (**2**)), produced by their dissociation, are shown on the right side of the same figure, ordered by increasing acidity values from top to bottom. Acidity was estimated on the basis of the energy (E_L) of the

Table 3. Reaction Energies (kcal/mol) for the Examined Reactions Calculated At LDA Level

(a) Dissociation of Cocatalytic Precursors

(1)	$[AlMe_3]2 \rightarrow 2AlMe_3$	+19.8
(2)	$Me_3Al{\cdot}MAO^H \rightarrow AlMe_3 + MAO^H$	+23.5

(b) Chlorine-Bridged Adduct Formation

		Mt = Ti	Mt = Zr
(3)	$Cp_2MtMeCl + AlMe_3 \rightarrow Cp_2MtMe{\cdot}ClAlMe_3$	−11.5	−6.6
(4)	$Cp_2MtMeCl + MAO^H \rightarrow Cp_2MtMe{\cdot}ClMAO^H$	−24.0	−22.0

(c) Free Cation Formation

		Mt = Ti	Mt = Zr
(0)	$Cp_2MtMeCl \rightarrow Cp_2MtMe^+ + Cl^-$	+160.9	+168.4
(5)	$Cp_2MtMe{\cdot}ClAlMe_3 \rightarrow Cp_2MtMe^+ + ClAlMe_3^-$	+124.3	+126.9
(6)	$Cp_2MtMe{\cdot}ClMAO^H \rightarrow Cp_2MtMe^+ + ClMAOH^-$	+101.9	+107.4
(8)	$Cp_2MtMe{\cdot}ClMAO^H{\cdot}AlH_2^+ \rightarrow Cp_2MtMe^+ + ClMAOH{\cdot}AlH_2$	+40.4	+44.0
(11)	$ClMAO^H{\cdot}MtCp_2Me \rightarrow Cp_2MtMe^+ + ClMAOH^-$	+122.9	+133.7
(12)	$MAO^H{\cdot}MtCp_2Me^+ \rightarrow Cp_2MtMe^+ + MAOH$	+52.8	+61.8

(d) Metallocene/Trimethyaluminum Exchange Reactions

		Mt = Ti	Mt = Zr
(9)	$Cp_2MtMe{\cdot}ClMAO^H{\cdot}AlMe_3 \rightarrow Me_3Al{\cdot}ClMAO^H{\cdot}MtCp_2Me$	+6.6	+1.5
(10)	$Cp_2MtMe{\cdot}ClMAO^H{\cdot}AlH_2^+ + MAOH{\cdot}AlMe_3 \rightarrow MAO^H{\cdot}MtCp_2Me^+ + Me_3Al{\cdot}ClMAO^H{\cdot}AlH_2$	+13.3	+7.9

(e) Ethylene Coordination

		Mt = Ti	Mt = Zr
(13)	$Cp_2MtMe^+ + C_2H_4 \rightarrow Cp_2MtMeC_2H_4^+$	−22.1	−28.8

(f) Trimethylaluminum/Counterion Reactions

(14)	$AlMe_3 + ClAlMe_3^- \rightarrow [AlMe_3]_2Cl^-$	−24.5
(15)	$AlMe_3 + ClMAO^{H-} \rightarrow Me_3Al{\cdot}ClMAO^{H-}$	−14.9
(16)	$AlMe_3 + ClMAO^HAlH_2 \rightarrow Me_3Al{\cdot}ClMAO^H{\cdot}AlH_2$	−9.4
(17)	$AlMe_3 + ClMAO^{H-} \rightarrow ClMAOH{\cdot}AlMe_3^-$	−43.5
(18)	$AlMe_3 + MAO^H \rightarrow MAOH{\cdot}AlMe_3$	−35.1

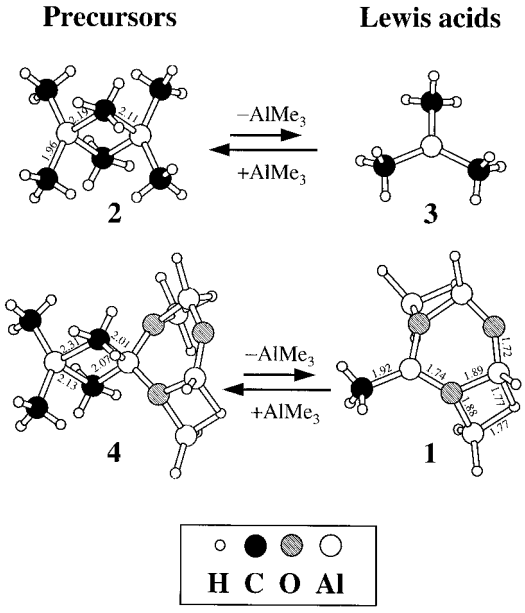

Figure 6. Optimized structures of $AlMe_3$ and MAO^H in associated (precursors **2** and **4** on the left) and dissociated (Lewis acids **3** and **1** on the right) forms.

lowest unoccupied molecular orbital (LUMO), obtained by DFT calculations: −1.627 and −2.547 eV respectively for $AlMe_3$, and MAO^H. The LUMO coincides with the empty p orbital of the tricoordinated Al atoms in $AlMe_3$ and MAO^H (Al*).

The net positive charge values of Al in $AlMe_3$ (+0.538 au), and of Al* in MAO^H (+0.665 au) follow the same trend of increasing Lewis acidity determined on the basis of the E_L values.

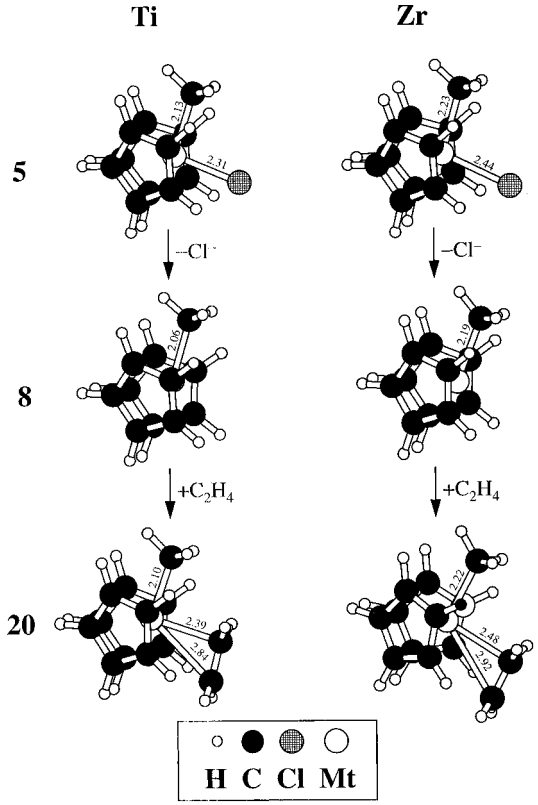

Figure 7. Optimized structures of titanium and zirconium bis(cyclopentadienyl) complexes: chloromethyl precursors (**5**), methylated cations (**8**), and ethylene complexes (**20**).

These results confirm the initial hypothesis that the tricoordinated oxygen atoms bound to Al* in MAO^H produce an electron-withdrawing effect, making this

Table 4. Binding Energies (kcal/mol) of the Examined Intermediates Calculated at the NLDA Level

Group A. Cocatalytic Precursors and Lewis Acids (Figure 6)		
2	$[AlMe_3]_2$	−2233.9
4	$Me_2Al[Me]_2Al[OAl_2H_4]_2O$	−2758.9
3	$AlMe_3$	−1113.0
1	$MeAl[OAl_2H_4]_2O$	−1635.7

Group B. Metallocene Complexes (Figure 7)			
		Me = Ti	Me = Zr
5	$Cp_2MtMeCl$	−2860.5	−2896.8
8	Cp_2MtMe^+	−2633.3	−2660.4
20	$Cp_2MtMe(C_2H_4)^+$	−3201.5	−3234.8

Group C. Chlorine-Bridged Metallocene/ Aluminum Adducts (Figures 8 and 11)			
		Mt = Ti	Mt = Zr
6	$Cp_2MtMe{\cdot}ClAlMe_3$	−3975.7	−4009.9
7	$Cp_2MtMe{\cdot}ClMeAl[OAl_2H_4]_2O$	−4508.8	−4543.3
12	$Cp_2MtMe{\cdot}ClMeAl[OAl_2H_4]_2O{\cdot}AlH_2^+$	−4552.9	−4585.9
14	$Cp_2MtMe{\cdot}ClMeAl[OAl_2H_4]_2O{\cdot}AlMe_3$	−5635.5	−5669.4

Group D. Chlorinated Counterions (Figure 9)		
9	$ClAlMe_3^-$	−1239.7
10	$ClMeAl[OAl_2H_4]_2O^-$	−1796.5
13	$ClMeAl[OAl_2H_4]_2O{\cdot}AlH_2$	−1905.6

Group E. Oxygen-Coordinated Metallocene/ Aluminum Adducts (Figures 10 and 11)			
		Mt = Ti	Mt = Zr
19	$ClMeAl[OAl_2H_4]_2O{\cdot}MtCp_2Me$	−4515.9	−4555.8
17	$MeAl[OAl_2H_4]_2O{\cdot}MtCp_2Me^+$	−4288.8	−4324.2
15	$Me_3Al{\cdot}ClMeAl[OAl_2H_4]_2O{\cdot}MtCp_2Me$	−5629.0	−5667.6

Group F. Trimethylaluminum Stabilized Counterions (Figure 12)		
21	$Cl[AlMe_3]_2^-$	−2369.8
22	$Me_3Al{\cdot}ClMeAl[OAl_2H_4]_2O^-$	−2914.0
18	$Me_3Al{\cdot}ClMeAl[OAl_2H_4]_2O{\cdot}AlH_2$	−3015.5
23	$ClMeAl[OAl_2H_4]_2O{\cdot}AlMe_3^-$	−2931.3
16	$MeAl[OAl_2H_4]_2O{\cdot}AlMe_3$	−2762.9
	Cl^-	−81.5
	C_2H_4	−560.8

aluminum atom more acidic than that in monomeric $AlMe_3$.

The accuracy of the calculated geometries is demonstrated by the good agreement observed between the calculated Al−C bond lengths in the dimeric trimethylaluminum and those obtained by crystallographic data:[30] 2.11−2.19 Å (calculated) vs 2.24 Å (experimental) for the Al−Me−Al bridging bonds and 1.96 Å (calculated) vs 2.00 Å (experimental) for the Al−Me terminal bonds.

The six-membered ring in the relaxed structure of MAO^H assumes a chair conformation and is characterized by a succession of nonequivalent Al−O bonds: in fact Al*−O bonds (1.74 Å) and Al−O* bonds (1.72 Å) are significantly shorter than the other Al−O bonds (1.88−1.89 Å) present in the molecule. The two aluminum atoms protruding out of the ring structure form Al−H−Al bridges, saturating their fourth coordinative valence. These structural features are peculiar to all of the MAO models examined in the present work.

Binding energies calculated for all the compounds represented in Figure 8 are reported in Table 2 (group A).

Metallocene Complexes

In Figure 7 the structures of $Cp_2MtMeCl$ chloroalkylated neutral precursors (**5**), Cp_2MtMe^+ cations (**8**) and $Cp_2MtMe(C_2H_4)^+$ ethylene complexes (**20**) are shown for both Ti and Zr. Their binding energies obtained by DFT calculations are reported in Table 2 (group B).

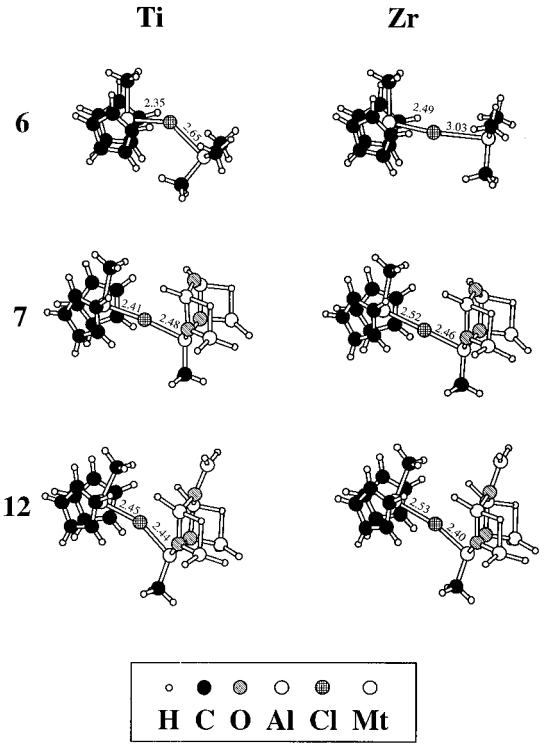

Figure 8. Optimized structures of titanium and zirconium chlorine-bridged metallocene/cocatalyst adducts: $Cp_2MtMe{\cdot}ClAlMe_3$ (**6**), $Cp_2MtMe{\cdot}ClMAO^H$ (**7**), and $Cp_2MtMe{\cdot}ClMAO^H{\cdot}AlH_2^+$ (**12**).

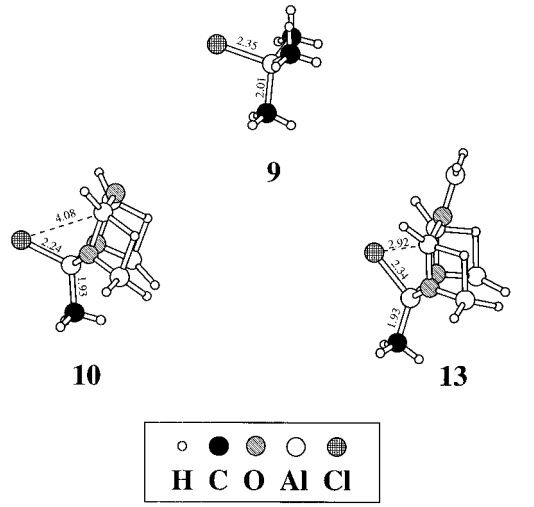

Figure 9. Optimized structures of $ClAlMe_3^-$ (**9**) and $ClMAO^{H-}$ (**10**) counterions and $ClMAO^H{\cdot}AlH_2$ "virtual anion" (**13**).

The structural features of these complexes are in close agreement with those obtained by experimental crystal data[31] and with those calculated by other authors[32] by quantum-mechanical calculations; therefore, they will not be the object of a detailed description.

The comparison of Mt−R bond lengths (R = Me, Cl, CH_2(olefin)) between homologous structures of the two metals reveals an average difference of about 0.11 Å, reflecting the difference of the ionic radii between titanium and zirconium.

The energies required to extract the chloride anion from $Cp_2MtMeCl$ are 160.9 kcal/mol for titanium and 168.4 kcal/mol for zirconium (Table 3, section c) while ethylene coordination energies to the free cations to form

Table 5. Reaction Energies (kcal/mol) for the Examined Reactions Calculated at the NLDA Level

(a) Dissociation of Cocatalytic Precursors

(1)	$[AlMe_3]_2 \rightarrow 2AlMe_3$	+7.9
(2)	$Me_3Al{\cdot}MAO^H \rightarrow AlMe_3 + MAO^H$	+10.2

(b) Chlorine-Bridged Adduct Formation

		Mt = Ti	Mt = Zr
(3)	$Cp_2MtMeCl + AlMe_3 \rightarrow Cp_2MtMe{\cdot}ClAlMe_3$	−2.2	−0.1
(4)	$Cp_2MtMeCl + MAO^H \rightarrow Cp_2MtMe{\cdot}ClMAO^H$	−12.6	−10.8

(c) Free Cation Formation

		Mt = Ti	Mt = Zr
(0)	$Cp_2MtMeCl \rightarrow Cp_2MtMe^+ + Cl^-$	+145.7	+154.9
(5)	$Cp_2MtMe{\cdot}ClAlMe_3 \rightarrow Cp_2MtMe^+ + ClAlMe_3^-$	+102.7	+109.8
(6)	$Cp_2MtMe{\cdot}ClMAO^H \rightarrow Cp_2MtMe^+ + ClMAOH^-$	+79.0	+86.4
(8)	$Cp_2MtMe{\cdot}ClMAO^H{\cdot}AlH_2^+ \rightarrow Cp_2MtMe^+ + ClMAOH{\cdot}AlH_2$	+14.0	+19.9
(11)	$ClMAO^H{\cdot}MtCp_2Me \rightarrow Cp_2MtMe^+ + ClMAOH^-$	+86.1	+98.9
(12)	$MAO^H{\cdot}MtCp_2Me^+ \rightarrow Cp_2MtMe^+ + MAOH$	+19.8	+28.1

(d) Metallocene/Trimethyaluminum Exchange Reactions

		Mt = Ti	Mt = Zr
(9)	$Cp_2MtMe{\cdot}ClMAO^H{\cdot}AlMe_3 \rightarrow Me_3Al{\cdot}ClMAO^H{\cdot}MtCp_2Me$	+6.5	+1.8
(10)	$Cp_2MtMe{\cdot}ClMAO^H{\cdot}AlH_2^+ + MAOH{\cdot}AlMe_3 \rightarrow MAO^H{\cdot}MtCp_2Me^+ + Me_3Al{\cdot}ClMAO^H{\cdot}AlH_2$	+11.5	+9.1

(e) Ethylene Coordination

		Mt = Ti	Mt = Zr
(13)	$Cp_2MtMe^+ + C_2H_4 \rightarrow Cp_2MtMeC_2H_4^+$	−7.4	−13.6

(f) Trimethylaluminum/Counterion Reactions

(14)	$AlMe_3 + ClAlMe_3^- \rightarrow [AlMe_3]_2Cl^-$	−17.1
(15)	$AlMe_3 + ClMAO^{H-} \rightarrow Me_3Al{\cdot}ClMAO^{H-}$	−4.5
(16)	$AlMe_3 + ClMAO^HAlH_2 \rightarrow Me_3Al{\cdot}ClMAO^H{\cdot}AlH_2$	+3.1
(17)	$AlMe_3 + ClMAO^{H-} \rightarrow ClMAOH{\cdot}AlMe_3^-$	−21.8
(18)	$AlMe_3 + MAO^H \rightarrow MAOH{\cdot}AlMe_3$	−14.2

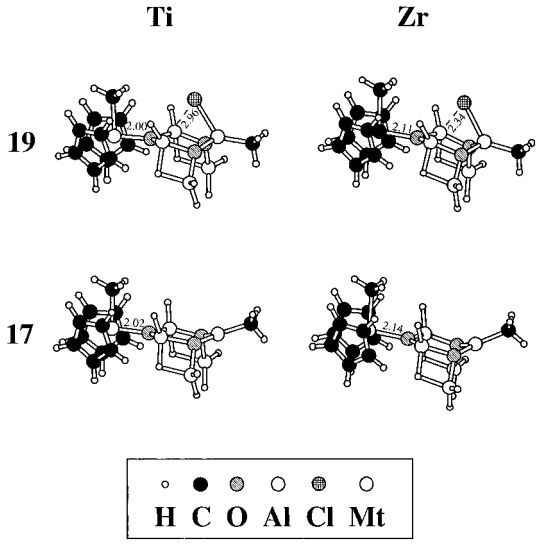

Figure 10. Optimized structures of titanium and zirconium oxygen-coordinated metallocene/cocatalyst adducts: $ClMAO^H{\cdot}MtCp_2Me$ (**19**) and $MAO^H{\cdot}MtCp_2Me^+$ (**17**).

$Cp_2MtMe(C_2H_4)^+$ complexes are respectively −22.1 kcal/mol for titanium and −28.8 kcal/mol for zirconium (Table 3, section e). These results suggest a higher affinity of the zirconocene cation toward nucleofilic species like Cl^- and C_2H_4, compared to the titanocene cation. Looking at the LUMO energies of the Cp_2MtMe^+ cations (−9.067 eV for titanium and −8.098 eV for zirconium), as a measure of their electronic affinity, the opposite behavior should be expected. Possible explanations are derived from the unfavorable coordinative situation of titanium compared to zirconium in metallocene complexes, due to the smaller ionic radius of this metal, combined with the presence of the two sterically hindering cyclopentadienyl rings, and by the lower value of its positive charge ($Q_{Ti} = +0.477$ au vs $Q_{Zr} = +0.616$ au).

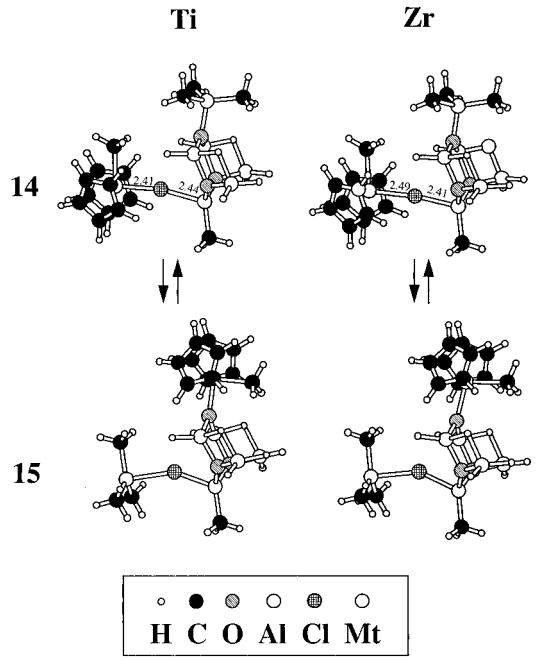

Figure 11. Optimized structures of titanium and zirconium metallocene/MAO^H/$AlMe_3$ adducts: $Cp_2MtMe{\cdot}ClMAO^H{\cdot}AlMe_3$ (**14**) and $Me_3Al{\cdot}ClMAO^H{\cdot}MtCp_2Me$ (**15**).

Chlorine-Bridged Metallocene/Cocatalyst Adducts

Reactions of metallocene precursors $Cp_2MtMeCl$ with $AlMe_3$ and MAO^H produce the chlorine-bridged Mt−Cl−

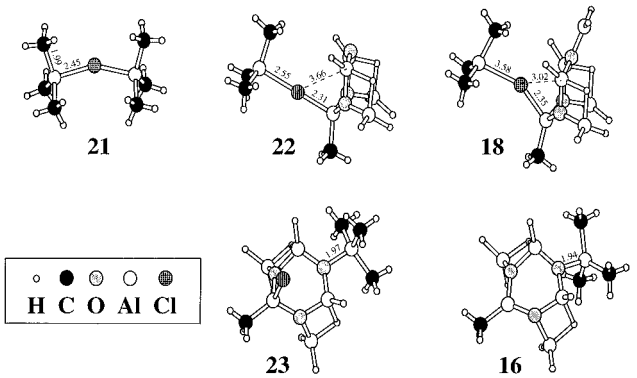

Figure 12. Chlorine-coordinated (top) and oxygen-coordinated (bottom) $AlMe_3$-stabilized counterions and "virtual anions": $[AlMe_3]_2Cl^-$ (**21**), $Me_3Al{\cdot}ClMAO^{H-}$ (**22**), $Me_3Al{\cdot}ClMAO^HAlH_2$ (**18**), $ClMAO^H{\cdot}AlMe_3^-$ (**23**), and $MAO^H{\cdot}AlMe_3$ (**16**).

Al adducts **6** and **7** shown in Figure 8 where the structure of adducts **12**, the precursors of the "virtual ion-pair", are also reported. They are ordered from top to bottom for increasing values of Lewis acidity of the tricoordinated aluminum atom of the cocatalytic precursor, and their binding energies are reported in Table 2 (group C).

Coordination of the trivalent aluminum atom of the cocatalyst to the chlorine atom of $Cp_2MtMeCl$ increases the polarization degree of the Mt−Cl bond. In fact, calculating the value of the electrostatic charge induced in the $Cp_2MtMe^{\delta+}$ moiety, as the sum (ΣQ_{Mt}) of the net charges of all $Cp_2MtMe^{\delta+}$ atoms in each adduct, we obtained the following results for the the two transition metal series: $\Sigma Q_{Ti} = +0.288, +0.409, +0.496$ au and $\Sigma Q_{Zr} = +0.298, +0.426, +0.495$ au, respectively, for the adducts with $AlMe_3$, MAO^H, and $MAO^H{\cdot}AlMe_2^+$. Furthermore, for both metal families, our calculations show that Mt−Cl bond lengths grow in the same order (Figure 10), with a parallel decrease of Cl−Al bond lengths.

These results clearly confirm the widely accepted idea[8] that the most efficient extractors of Cl^- anions from metallocene precursors are cocatalyts characterized by a strong Lewis acidity.

Counterions and "Virtual Anions"

The heterolytic dissociation of Mt−Cl bonds in the adducts **6**, **7**, and **12** leads to the formation of ion pairs where the cationic moieties are the Cp_2MtMe^+ complexes (Figure 7) and the correspondent counteranions are respectively $ClAlMe_3^-$ (**9**), $ClMAO^{H-}$ (**10**), and the $ClMAO^H{\cdot}AlH_2$ "virtual anion" (**13**): their optimized structures are shown in Figure 9, while their binding energies are reported in Table 2 (group D).

The Cl−Al* bond in $ClMAO^{H-}$ is shorter than the Cl-Al bond in $ClAlMe_3^-$, as a consequence of the electron-withdrawing effect performed by the tricoordinated oxygen atoms bound to Al*. In $ClMAO^H{\cdot}AlH_2$, the Cl−Al* bond is longer than in $ClMAO^{H-}$, because of the stabilizing interactions occurring between Cl and the other two Al atoms of the six-membered ring (Cl−Al = 2.92 Å). Such stabilizing interactions are probably induced by the presence of the AlH_2^+ moiety coordinated to O* and are absent in $ClMAO^{H-}$ (Cl−Al = 4.08 Å).

The negative charge on Cl atom decreases in the order $ClAlMe_3^-$ (-0.420 a.u.), $ClMAO^{H-}$ (−0.302 au), and $ClMAO^H{\cdot}AlH_2$ (−0.159 au). A less evident parallel decrease of the methyl carbon negative charge was also observed (−0.310, −0.289, and −0.263 au respectively for **9**, **10**, and **13**).

Oxygen-Coordinated Metallocene/MAO^H Adducts

The optimized structures of the oxygen coordinated $ClMAO^H{\cdot}MtCp_2Me$ (**19**) and $MAO^H{\cdot}MtCp_2Me^+$ (**17**) adducts are shown respectively at the top and bottom of Figure 10; calculated binding energies of these compounds are reported in Table 2 (group D).

In both kinds of adducts the difference between Ti−O and Zr−O bond lengths clearly reflects the values of the ionic radius of the two metals. In **19** (Figure 10, top, right) the Zr−O bond length (2.11 Å) is in good agreement with experimental structural data (2.044 Å) obtained by Erker et al.[21b] for $[Cp_2Zr(Me)OAlMe_2]_2$. In both adducts **19**, the coordination of Cp_2MtMe^+ to O* induces a partial coordination of the chlorine atom to the two Al atoms bonded to O*, in close analogy with that observed in the case of $ClMAO^H{\cdot}AlH_2$.

Metallocene/MAO^H/$AlMe_3$ Adducts

In Figure 11 the structures of the two kinds of $Cp_2MtMe^+/ClMAO^{H-}/AlMe_3$ adducts **14** and **15**, used to study the thermodynamics of the exchange reaction between the metallocene cation and $AlMe_3$ on the small size $ClMAO^{H-}$ counterion (reaction 10) are reported. The relative binding energies calculated with DFT method are reported in Table 2 (group C and group E). The almost planar configuration of $AlMe_3$ in **15** implies that this molecule is only weakly coordinated to the Cl atom, which is already involved in quite strong interactions with the two Al atoms bonded to O*.

$AlMe_3$-Stabilized Counterions and "Virtual Anions"

In Figure 12 the structure and main geometrical parameters of the different $AlMe_3/MAO^H$ adducts are examined, i.e., the three chlorine bridged trimethyaluminum/chlorinated-counterion adducts **21**, **22**, and **23** (top) and the oxygen-coordinated adducts **16** and **23** (bottom). The relative binding energies are reported in Table 2 (group F).

The coordination of $AlMe_3$ to the chlorine atom of $ClAlMe_3^-$ to form $Cl[AlMe_3]_2^-$ causes an increase of the Al−Cl bond length from 2.35 to 2.45 Å. In a similar way in $Me_3Al{\cdot}ClMAO^{H-}$ the Cl-Al* bond length is increased from the value of 2.24 Å of $ClMAO^{H-}$ to 2.31 Å, while the Me_3Al−Cl bond is remarkably longer (2.55 Å). The interaction between $AlMe_3$ and $ClMAO^H{\cdot}AlH_2$ to form **18** can be considered as a purely nonbonded interaction (Me_3Al−Cl = 3.58 Å). This observation is also supported by $AlMe_3$ complexation energy values calculated for reactions 14−16 and is reported in section f of Table 3. These data indicate that $AlMe_3$ coordination to the chlorinated counterions is closely related to their ability to delocalize the negative charge on the Cl atom: in fact the lowest complexation energy (−9.4 kcal/mol) is obtained in the case of $ClMAO^H{\cdot}AlH_2$ "virtual anion" where Q_{Cl} is only −0.159 au, and the highest value (−24.5 kcal/mol) is observed in the case of $ClAlMe_3$ where Q_{Cl} is −0.420 au.

Higher values of $AlMe_3$ complexation energy were obtained for oxygen-coordinated adducts **23** and **16** (Table 3, section f, reactions 17 and 18): as expected the highest value (−43.5 kcal/mol) is observed in the case of coordination to $ClMAO^{H-}$ anion, where the negative charge on O* is −0.474 au; it is reduced to −35.1 kcal/mol in the case of the neutral MAO^H where Q_{O^*} is −0.462 au. These results also explain why the

O*−$AlMe_3$ bond length is longer in **16** (1.94 Å) than in **23** (1.91 Å).

Thermodynamics of Active Species Formation

The reactions

$$Cp_2MtMeCl + {}^1/_2[AlMe_3]_2 \rightarrow Cp_2MtMe{\cdot}ClAlMe_3 \quad (19)$$

$$Cp_2MtMeCl + Me_3Al{\cdot}MAO^H \rightarrow Cp_2MtMe{\cdot}ClAO^H + {}^1/_2[AlMe_3]_2 \quad (20)$$

include the dissociation of the two cocatalytic precursors, $[AlMe_3]_2$ and $Me_3Al{\cdot}MAO^H$, to form the correspondent Lewis acids $AlMe_3$ and MAO^H (Table 3, section a) and their reaction with $Cp_2MtMeCl$ to give the chlorine-bridged adducts (Reactions 5 and 6 in Table 3, section b).

In the case of trimethylaluminum, our calculations show that reaction 19 is slightly exothermic for titanium (−1.6 kcal/mol) and moderately endothermic for zirconium (+3.3 kcal/mol).

The reactions of titanium and zirconium metallocenes with $Me_3Al{\cdot}MAO^H$ are remarkably exothermic in both cases (−10.4 and −8.4 kcal/mol, respectively), confirming that MAO^H is more reactive toward the metallocenes. The comparative behavior of the two metals in reactions 19 and 20 shows that the formation of the titanium-based adducts is always favored with respect to the zirconium-based ones.

Dissociation of Chlorine-Bridged Adducts

The next step consists of the study of the dissociation of these adducts to form free cation/anion pairs through Mt−Cl bond breaking. Section C of Table 3 shows that, for reactions 5 and 6, the energies required to dissociate the Mt−Cl bond in $Cp_2MtMe{\cdot}ClAlMe_3$ and $Cp_2MtMe{\cdot}ClMAO^H$, although remarkably lower than those required in the case of $Cp_2MtMeCl$ precursors (reaction 0), are always higher than 100 kcal/mol.

With $MAO^H{\cdot}AlH_2^+$ model, as described by reaction 8, no charge separation occurs and dissociation energies (+40.4 and +44.0 kcal/mol respectively for titanium and zirconium) are remarkably lower than those calculated for the metallocene adducts with $AlMe_3$ and MAO^H. These results confirm that an efficient delocalization of the negative charge of the anion, which in this case has been simulated by its complete neutralization, is essential to obtain a significative reduction of the ion-pair separation energy.

It is noteworthy that, also in this extremely favorable case, the energy required to form free metallocene cations is on the order of 40 kcal/mol, a value always too high to justify the high polymerization rates experimentally observed with metallocene/MAO systems. In fact the intermittent chain-growth scheme proposed by Fink and co-workers[33] and sketched in Figure 13 implies separation of ion-pairs at each monomer insertion step: consequently the ion-pair dissociation energy should be of the same order of magnitude of the activation energy in the propagation step, whose experimental value is about 7 kcal/mol.[34]

Cation Solvation

Because we performed our calculations in a vacuum, their major limitation consists of neglecting the contribution of ion solvation. As mentioned in the Introduction, the experimental solvation energies estimated for toluene solutions of cationic metallocenes are 15−30 kcal/mol.[11] We assumed that the main contribution to the solvation energy difference between the Cp_2MtX_2 neutral complex and the Cp_2MtX^+ cationic complex arises from the interaction of the latter with a solvent molecule S, which coordinates to the transition metal atom forming the $Cp_2MtX(S)^+$ complex, where the outer solvation shell remains substantially unaltered. In this framework, it is not unreasonable to think that the coordination energy of an ethylene molecule to the free metallocenic cation is of the same order of magnitude as that of an aromatic solvent. From Table 3 (section e) we see that the ethylene coordination energy is −22.1 kcal/mol in the case of titanium and −28.8 kcal/mol for zirconium, values that fall in the experimental range. Therefore, assuming that olefin coordination energy roughly reproduces the solvation energy, the formation of monomer-stabilized virtual ion pairs $Cp_2MtMe(C_2H_4)^+/ClMAO^H{\cdot}AlH_2$ require 18.3 kcal/mol for titanium and 15.2 kcal/mol for zirconium; these results are in closer agreement with the experimental free energy values for the propagation reaction. Although it is important to remark that these considerations are purely thermodynamic in nature and that kinetic aspects could further penalize ion pair separation, the calculated energies are expected to further decrease, taking into account the interactions occuring between the cationic $Cp_2MtMe(C_2H_4)^+$ complex and the counterion, when the formation of olefin separated ion pairs (OSIP) is admitted. In fact, in a previous paper,[10] we emphasized that the formation of OSIP intermediates, where an olefin molecule is sandwiched between the cation and anion, represents the most feasible polymerization mechanism for the $Cp_2TiMeCl/AlMe_2Cl$ system. In that case the barrier to olefin coordination drops down from 90 to about 30 kcal/mol. In the case of $Cp_2MtMe(C_2H_4)^+/ClMAO^H{\cdot}AlH_2$, it is expected to be reduced to a few kilocalories per mole. The study of these systems is in progress and will be the object of a future paper.

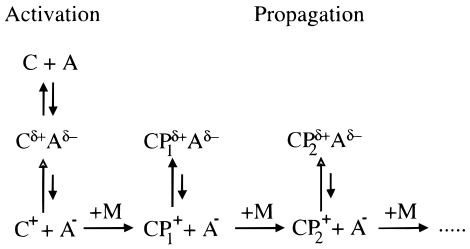

Figure 13. Multiple equilibria scheme of polymerization process: C = catalyst precursor; A = cocatalyst; $C^{\delta+}A^{\delta-}$ = polarized complex; C^+ = cationic species; A^- = counterion; M = monomer; P_i = growing polymer chain; i = number of inserted monomeric units.

Counterion Stabilization Induced by $AlMe_3$

In principle, a further stabilization effect could arise from $AlMe_3$ coordination to the residual chlorine atom bound to MAO (Table 3, section e, reactions 14−16), but this contribution appears to be negligible (+0.5 kcal/mol) in the less unfavorable case of dissociation of $Cp_2MtMe{\cdot}ClMAO^H{\cdot}AlH_2^+$, if the energy required to dissociate $[AlMe_3]_2$ dimer is also taken into account.

Oxygen-Coordinated Adducts

As mentioned in the Introduction, the migration of Cp_2MtMe^+ cation along the alumoxane chain to form oxygen-bridged metallocene/MAO adducts both for the

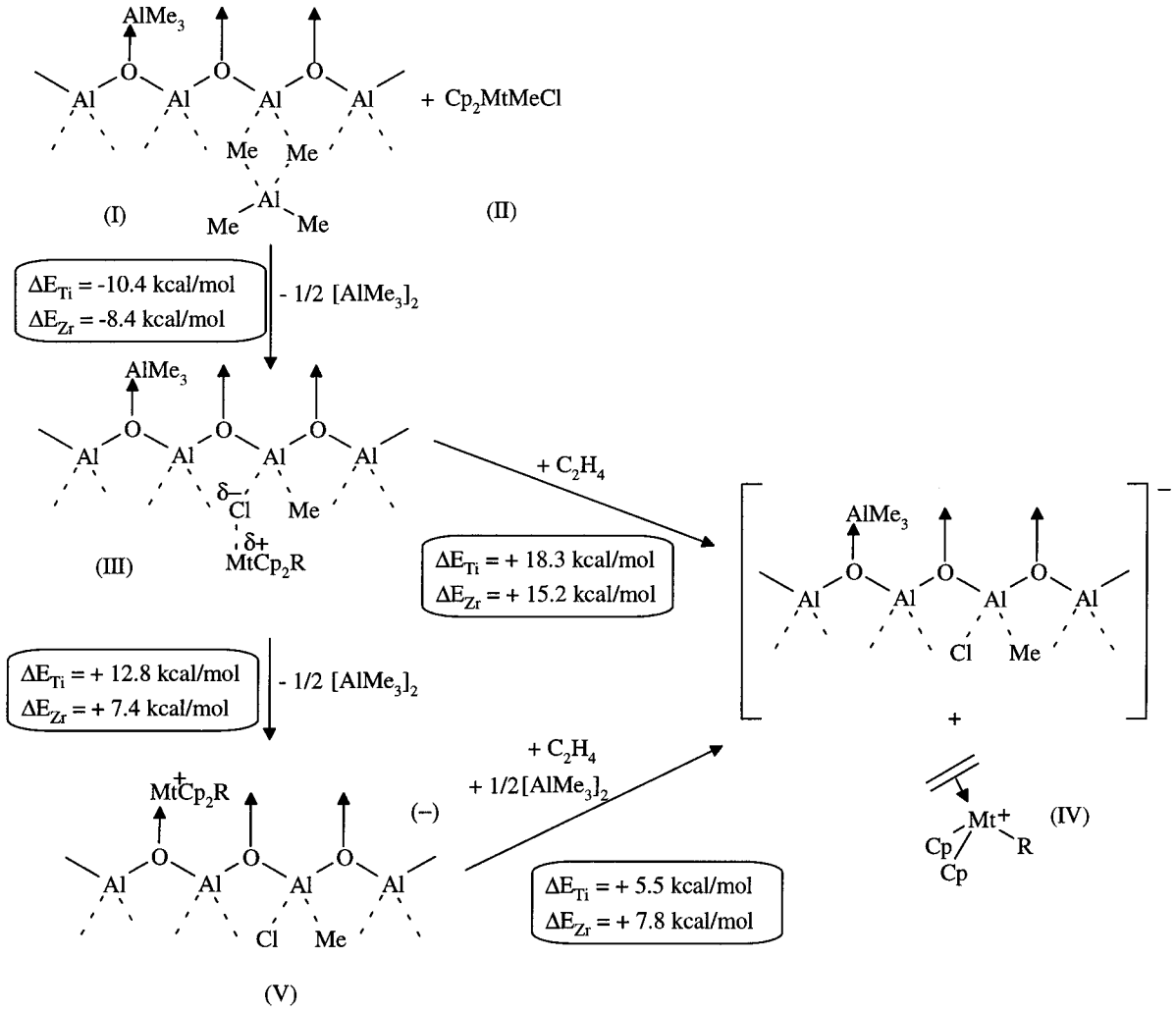

Figure 14. Reaction scheme between metallocene and MAO: MAO (**I**) and chloroalkylated metallocene (**II**) react to form chlorine-bridged adducts (**III**) that, in the presence of olefinic monomers, can dissociate to form metastable cationic species (**IV**) which undergo olefin insertion. At high Al/Mt ratios cationic metallocenes can react with oxygen atoms of alumoxanic chains to form oxygen-coordinated adducts (**V**) that, in the presence of monomer and $AlMe_3$, can dissociate to form metastable active species (**IV**). The energetics of the reactions involving both titanium- and zirconium-based complexes is reported, for the case of a virtual infinitely-large $XMAO^-$ macroanion.

small size MAO^H model (reaction 9) and for a virtual infinitely large macroanionic MAO model (reaction 10) is flanked by migration of $AlMe_3$ from oxygen to chlorine atom in the opposite direction (Table 3, Section c). In both cases such a migration is thermodynamically unfavorable: in the case of small size MAO model, it is less difficult for zirconium (+1.4 kcal/mol) than for titanium (+6.6 kcal/mol). An analogous situation occurs for reaction 10, which appears to be even more endothermic (+13.3 and +7.9 kcal/mol for titanium and zirconium, respectively).

The slight ability of the small $Me_3Al{\cdot}ClMAO^{H-}$ counterion to delocalize the negative charge causes the high dissociation energy values calculated for the Mt−O bond breaking for both metals (+118.9 kcal/mol for titanium and +128.5 kcal/mol for zirconium). A remarkable decrease of these energies is observed in the case of the dissociation of the $MAO^H{\cdot}Cp_2MtMe^+$adducts. Because no charge separation occurs in this case, Mt−O bond dissociation energies decrease to +52.8 kcal/mol for titanium and +61.8 kcal/mol for zirconium.

If the stabilizing effect of monomer coordination to cationic metallocenes (reaction 13) is taken into account, the energy to dissociate the $MAO^H{\cdot}Cp_2MtMe^+$ virtual ion pair to form the $MAO^H/Cp_2MtMe(C_2H_4)^+$ pair becomes +30.7 kcal/mol for titanium and +33.0 kcal/mol for zirconium. A further energy contribution to the dissociation can arise from $AlMe_3$ coordination to O* in MAO^H to form the $MAO^H{\cdot}AlMe_3$ stabilized "virtual counterion". Different from the previously analyzed case of $Cl-AlMe_3$ interaction (reaction 16), the formation of an Al−O bond produces a nonnegligible stabilization effect: including all the contributions due to ethylene coordination to metallocenic cation, $[AlMe_3]_2$ dissociation, and $AlMe_3$ coordination to MAO^H, the energy required to obtain the $Cp_2MtMe(C_2H_4)^+/MAO^H{\cdot}AlMe_3$ pair becomes +5.5 kcal/mol for titanium and +7.8 kcal/mol for zirconium. Although this mechanism seems feasible from a thermodynamic point of view, it should imply the simultaneous coordination of the olefin to the transition metal atom and $AlMe_3$ coordination to that oxygen atom: a situation that appears quite unrealistic to occur. For this reason we think that also in this case olefin coordination via OSIP species should be considered the most feasible polymerization mechanism.

A side result coming from the comparison of the energetics of reactions 18 and 2 is that the coordination of monomeric $AlMe_3$ to O* to form adduct **4** is favored (−35.1 kcal/mol) with respect to the formation of the dimethyl-bridged adduct **3** (−23.5 kcal/mol), confirming

the hypothesis discussed in the presentation of MAO models.

Comparison between Titanium and Zirconium

The different behaviors of titanium and zirconium complexes can be rationalized by analyzing the dissociation energy of the correspondent chlorine-bridged and oxygen-coordinated metallocene/MAO adducts reported in Table 3 (section c): Zr−X bonds (X = Cl, O) are always stronger than correspondent Ti−X bonds, but the energy difference between the two metals is higher for Mt−O bonds.

General Reaction Scheme

In Figure 14 a general scheme summarizing the thermodynamics of the reactions supposed to be involved in active species formation is presented. From this scheme we can infer the following considerations:

The first product obtained by mixing MAO (**I**) with a metallocene (**II**) is the chlorine-bridged polarized adduct (**III**).

In the presence of olefins such an adduct can dissociate to form cationic species (**IV**) able to undergo olefin insertion (polymerization).

At a high Al/Mt ratio and high temperature the formation of oxygen-stabilized adducts (**V**) is expected.

In the presence of olefins, adducts (**V**) can dissociate to form cationic active species (**IV**).

The formation of oxygen-stabilized adducts is expected to be easier for zirconium than for titanium-based metallocenes.

The presence of two kinds of "precatalytic" species (**III** and **V**) accounts for bimodal molecular weight and comonomer distributions observed in homo- and copolymerization of ethylene with the Cp_2ZrCl_2/MAO system under appropriate conditions;[35] electron-donor substituents on cyclopentadienyl rings are expecetd to stabilize the positive charge of the cationic species, favoring their migration along alumoxane chains with almost exclusive formation of oxygen-stabilized metallocene−MAO species (**V**).

$AlMe_3$ appears to be involved in almost all the reactions described.

Conclusions

The theoretical investigations of reactions between typical metallocene precursors and different cocatalytic site models of MAO has allowed us to reach some significant insights on the mechanisms involved in the formation of active species responsible for olefin polymerization:

The presence of highly acidic aluminum atoms in MAO can explain its higher cocatalytic activivity compared to $AlMe_3$.

Ion-pair dissociation is a difficult process whose energetics is not compatible with experimental polymerization data.

Negative charge dispersion in MAO macroanions strongly affects the ion-pair dissociation energy, reducing its value from more than 100 to about 40 kcal/mol; however, this feature cannot justify by itself the formation of free cationic species.

The stabilization of metallocene cations performed by monomer coordination to the transition metal plays an essential role in ion-pair separation, but according to our previous calculations[10] and to Brintzinger's hypothesis,[8b] it is expected that the formation of olefin separated ion pairs represents a more suitable model for the polymerization mechanism.

The presence of moderately coordinating oxygen atoms in MAO can be determinant in the cationic species stabilization, but also in this case, the OSIP model should be invoked to justify the high catalytic activity of methylalumoxane.

The $AlMe_3$ content in MAO can play an important role in determining its cocatalytic activity, both protecting the acidic cocatalytic sites as well as affecting the formation of stabilized Cp_2MtMe^+-O adducts.

The comparative analysis of the behavior of titanocenes and zirconocenes put into evidence that chlorine-bridged adducts with MAO are more easily formed with titanium than with zirconium, but the formation of olefin-stabilized titanium cations appears to be unfavored with respect to zirconium ones (reaction III → IV in Figure 14). At high Al/Mt ratio (reaction V → IV in Figure 14) the situation is inverted. These results do not justify the higher catalytic activity experimentally exhibited by zirconium-based catalysts (60 900 kg of PE/(mol of Mt·h·[Et])) compared to titanium based ones (34 200 kg of PE/(mol of Mt·h·[Et]))[8c]. However, it is well-known that, different from zirconium, titanium complexes can easily undergo side reactions like the formation of Ti^{III} adducts with $AlMe_3$[36] and Tebbe's reagent[37] which are not active in olefin polymerization. In absence of degradation reactions the two metals should exhibit a comparable catalytic activity with MAO. At high temperature and a high Al/Mt ratio deactivation of titanium complexes probably penalizes this metal with respect to zirconium. With $AlMe_3$ at a low Al/Mt ratio, only titanocene complexes are known to be active in ethylene polymerization. This observation can be justified assuming that the Mt−Cl bond breaking becomes the rate-determining step, favoring titanium vs zirconium.

References and Notes

(1) (a) Breslow, D. S.; Newburg, N. R. *J. Am. Chem. Soc.* **1957**, *79*, 5072−5072. (b) Natta, G.; Pino, P.; Mazzanti, G.; Giannini, U. *J. Am. Chem. Soc.* **1957**, *79*, 2975.

(2) (a) Ziegler, K.; Holzkamp, E.; Breil, H.; Martin, H. *Angew. Chem.* **1955**, *67*, 541. (b) Natta, G.; Pino, P.; Corradini, P.; Danusso, F.; Mantica, E.; Mazzanti, G.; Moraglio, G. *J. Am. Chem. Soc.* **1955**, *67*, 426. (c) Natta, G. *Atti Acc. Naz. Lincei Mem. Classe Sci. Fis. Mat. Nat. Sez. II* **1955**, *4*, 61.

(3) Sinn, H.; Kaminsky, W. *Adv. Organomet. Chem.* **1980**, *18*, 99.

(4) For a comprehensive collection of papers on this topic, see: *Macromol. Symp.* **1995**, *97*.

(5) Kaminsky, W. *Macromol. Symp.* **1995**, *97*, 79.

(6) (a) Cam, D.; Giannini, U. *Makromol Chem.* **1992**, *193*, 1049. (b) Sishta, C.; Hathorn, R. M.; Marks, T. J. *J. Am. Chem. Soc.* **1992**, *114*, 1112. (c) Tritto, I.; Li, S.; Sacchi, M. C.; Zannoni, G. *Macromol.* **1993**, *26*, 7111. (d) Tritto, I.; Sacchi, M. C.; Li, S. *Macromol. Rapid. Commun.* **1994**, *15*, 217.

(7) (a) Dyachkovskii, F. S.; Shilova, A. K.; Shilov, A. E. *J. Polym. Sci., Part C* **1967**, *16*, 2333. (b) Eisch, J. J.; Piotrowsky, A. M.; Brownstein, S. K.; Gabe, E. J.; Lee, F. L. *J. Am. Chem. Soc.* **1985**, *107*, 7219. (c) Gassman, P. G.; Callstrom, M. R. *J. Am. Chem. Soc.* **1987**, *109*, 7875. (d) Jordan, R. F.; Dasher, W. E.; Echols, S. F. *J. Am. Chem. Soc.* **1986**, *108*, 1718. (e) Yang, X.; Stern, C. L.; Marks, T. J. *J. Am. Chem. Soc.* **1991**, *113*, 3623. (f) Bochmann, M.; Lancaster, S. J.; *J. Organomet. Chem.* **1992**, *434*, C1. (g) Yang, X.; Stern, C. L.; Marks, T. J. *J. Am. Chem. Soc.* **1994**, *116*, 1015.

(8) (a) Barron, A. R. *Macromol. Symp.* **1995**, *97*, 15. (b) Brintzinger, H. H.; Fischer, D.; Mulhaupt, R.; Rieger, B.; Waymouth, R. M. *Angew. Chem., Int. Ed. Engl.* **1995**, *34*, 1143. (c) Kaminsky, W. *Macromol. Chem. Phys.* **1996**, *197*, 3907.

(9) Fusco, R.; Spera, S.; Longo, L.; Proto, A.; Abis, L.; Accomazzi, P.; Gila, L.; Guarini, A.; Bertoni, S.; Busetto, C.; Garbassi F. *Proceedings of 2nd International Congress on Metallocene*

Polymers; Schotland Business Research Inc.: Dusseldorf, Germany, 1996; p 335.
(10) Fusco, R.; Longo, L.; Masi, F.; Garbassi, F. *Macromol. Rapid Commun.* **1997**, *18*, 433.
(11) Richardson, D. E.; Alameddin, N. G.; Rayan, M. F.; Hayes, T.; Eyler, J. R.; Siedle, A. R. *J. Am. Chem. Soc.* **1996**,*118*, 11244.
(12) Sinn, H. *Macromol. Symp.* **1995**, *97*, 27.
(13) Pasynkiewicz, S. *Polyhedron* **1990**, *9*, 429.
(14) (a) Eisch, J. J. In *Comprehensive Organometallic Chemistry;* Wilkinson, G., Ed., Pergamon Press: Oxford, England 1982; Vol. 1, p 555. (b) Healy, D. M.; Power, M. B.; Barron, A. R., *Coord. Chem. Rev.* **1994**, *130*, 63.
(15) Siedle, A. R.; Lamanna; W. M., Olofson, J. M.; Nerad, B. A.; Newmark, R. A. In *Selectivity in Catalysis;* ACS Symposium Series 517; American Chemical Society: Washington, DC, 1993; p 156.
(16) Barron, A. R.; Dobbs, K. D.; Francl, M. M. *J. Am. Chem. Soc.* **1991**, *113*, 39.
(17) Sugano, T.; Matsubara, K.; Fujita, T.; Takahashi, T. *J. Mol. Catal.* **1993**, *82*, 93.
(18) (a) Resconi, L.; Bossi, S.; Abis, L. *Macromolecules* **1990**, *23*, 4489. (b) Michiels, W.; Munoz-Escalona, A. *Macromol. Symp.* **1995**, *97*, 171. (c) Srinivasa Reddy, S.; Radhakrishnan, K.; Sivaram, S. *Polym. Bull.* **1996**, *36*, 165. (d) Chien, J. C. W.; Wang, B. P. *J. Polym. Sci., Part A: Polym. Chem.* **1988**, *26*, 3089.
(19) Tritto, I.; Sacchi, M. C.; Locatelli, P.; Li, S. X. *Macromol. Symp.* **1995**, *97*, 101.
(20) Siedle, R. A.; Newmark, R. A.; Lamanna, W. M.; Schroepfer, J., N.; *Polyhedron* **1990**, *9*, 301.
(21) (a) Giannetti, E.; Nicoletti, G. M.; Mazzocchi, R. *J. Polym. Sci., Part A: Polym. Chem.* **1985**, *23*, 2117. (b) Erker, G.: Albrecht, M.; Werner, S.; Kruger, C. *Naturforsch., B.* **1990**, *45*, 1205.
(22) Cossee, P. *J. Catal.* **1964**, *3*, 80.
(23) DMol 4.0.0 by Molecular Simulations Inc. **1996**.
(24) (a) Delley, B. *Chem. Phys. Lett.* **1986**, *110*, 329. (b) Delley, B. *J. Chem. Phys.* **1986**, *92*, 508. (c) Delley, B. *J. Chem. Phys.* **1991**, *94*, 7245.
(25) (a) Press, W. H.; Flannery, B. P.; Teukolsky, S. A.; Vetterling, W. T. *Numerical Recipes, the Art of Scientific Computing*; Cambridge University Press: New York, 1986. (b) Pulay, P. *J. Comput. Chem.* **1982**, *3*, 556. (c) Csa'sza'r, P.; Pulay, P. *J. Mol. Struct.* **1984**, *114*, 31.
(26) Vosko, S. J.; Wilk, L.; Nusair, M. *Can. J. Phys.* **1980**, *58*, 1200.
(27) (a) Perdew, J. P.; Wang, Y. *Phys. Rev. B: Condens. Matter* **1992**, *45*, 13244. (b) Becke, A. D. J. *Chem. Phys.* **1988**, *88*, 2547.
(28) Busfield, W. Heats and Entropies of Polymerization, Ceiling Temperatures, Equilibrium Monomer Concentrations and Polymerizability of Heterocyclic Compounds. In *Polymer Handbook*, 3rd ed.; Brandrup, K. J.; Immergut, E. H., Eds.; J. Wiley & Sons: New York, 1989; p. II/297.
(29) Smith, M. B. *J. Organomet. Chem.* **1974**, *70*, 13.
(30) Lewis, P. H.; Rundle, R. E. *J. Chem. Phys.* **1953**, *21*, 986.
(31) (a) Clearfield, A.; Warner, D. K.; Saldarriaga-Molina, C. H.; Ropal, R.; Bernal, I. *Can. J. Chem.* **1975**, *53*, 1622. (b) Thewalt, U.; Wöhrle, T. *J. Organomet. Chem.* **1994**, *464*, C17. (c) Prout, K.; Cameron, T. S.; Forder, R. A.; Critchley, S. R.; Denton, B.;Rees, G. V. *Acta Crystallogr.* **1974**, *B30*, 2290. (d) Jordan, R. F.; Chandrasekhar, S. B.; Willet, R.; Scott, B. *J. Am. Chem. Soc.* **1986**, *108*, 7410.
(32) (a) Kawamura-Kuribayashi, H.; Koga, H.; Morokuma, K. *J. Am. Chem. Soc.* **1992**, *114*, 8687. (b) Woo, T. K.; Fan. L.; Ziegler, T. *Organometallics* **1994**, *13*, 2252
(33) Fink, G.; Fenzl, W.; Mynott, R. *Z. Naturforsch.* **1985**, *40B*, 158.
(34) Chien, J. C.; Razavi, A. J. *J. Polym. Sci., Part A: Polym. Chem.* **1988**, *26*, 2369.
(35) Vela Estrada, J. M.; Hamielec, A. E. *Polymer* **1994**, *35*, 808. (b) Soga, K.; Uozumi, T.; Arai, T.; Nakamura, S. *Macromol. Rapid Commun.* **1995**, *16*, 379. (c) Katayama, H.; Shiraishi, H.; Hino, T.; Takuya, O.; Imai, A. *Macromol. Symp.* **1995**, *97*, 109.
(36) Eisch, J. J.; Pombrik, S. I.; Zheng, G. *Organometallics* **1993**, *12*, 3856.
(37) (a) Ott, K. C.; deBoer, E. J. M.; Grubbs, R. H. *Organometallics* **1984**, *3*, 223. (b) Tebbe, F. N.; Parshall, G. W.; Ovenall, D. W. *J. Am. Chem. Soc.* **1978**, *100*, 3611.

MA9708611